

Influence of hydraulic property correlation on predicted dense nonaqueous phase liquid source zone architecture, mass recovery and contaminant flux

Lawrence D. Lemke

Department of Geology, Wayne State University, Detroit, Michigan, USA

Linda M. Abriola

Department of Civil and Environmental Engineering, Tufts University, Medford, Massachusetts, USA

John R. Lang

Department of Civil and Environmental Engineering, University of Michigan, Michigan, USA

Received 30 January 2004; revised 11 June 2004; accepted 19 August 2004; published 29 December 2004.

[1] Organic liquid saturation distributions resulting from a simulated tetrachloroethene (PCE) spill were generated with alternative models of spatially varying aquifer properties for a statistically homogeneous, nonuniform sand aquifer. The distributions were analyzed to quantify DNAPL source zone characteristics and then incorporated as initial conditions for simulated PCE recovery using surfactant-enhanced aquifer remediation (SEAR). The predicted evolution of the spatial distribution of DNAPL saturations or source zone “architectures” and associated remediation efficiencies are strongly influenced by the spatial correlation of aquifer parameters and multiphase flow constitutive relationships. Model predictions suggest that removal of 60 to 99% of entrapped PCE can reduce dissolved contaminant concentration and mass flux under natural gradient conditions by approximately two orders of magnitude. Aqueous phase contaminant flux, however, does not vary consistently as a function of the percentage of DNAPL removed, and notable differences in flux evolution were observed for models incorporating correlated versus uncorrelated capillary entry pressure and permeability fields. Simulation results demonstrate that the application of alternative models of aquifer parameter spatial variability can influence predicted DNAPL infiltration, entrapment, and recovery, even for relatively homogeneous aquifers of the type investigated here. Results also demonstrate potential benefits, in the form of reduced mass flux, accruing from partial mass removal that may not be readily predicted from analyses relying on simplified conceptual models for DNAPL source zone architecture or aquifer flow fields. *INDEX TERMS*: 1829 Hydrology: Groundwater hydrology; 1832 Hydrology: Groundwater transport; 1831 Hydrology: Groundwater quality; *KEYWORDS*: contamination mass flux, DNAPL remediation, DNAPL source zone, heterogeneity, nonuniformity

Citation: Lemke, L. D., L. M. Abriola, and J. R. Lang (2004), Influence of hydraulic property correlation on predicted dense nonaqueous phase liquid source zone architecture, mass recovery and contaminant flux, *Water Resour. Res.*, 40, W12417, doi:10.1029/2004WR003061.

1. Introduction

[2] Many groundwater contaminant plumes originate from portions of aquifers containing separate, dense nonaqueous phase liquids (DNAPLs), often referred to as “source zones.” Laboratory experiments and field studies have demonstrated that within such source zones, DNAPL can be widely distributed in pools, ganglia, and blobs [Schwille, 1988; Poulsen and Kueper, 1992; Powers *et al.*, 1992; Kueper *et al.*, 1993; Feenstra *et al.*, 1996]. The presence of pooled or residual DNAPL is difficult to detect in the subsurface, yet can create a persistent dissolved

contaminant source that may be hydraulically contained but not readily removed by traditional pump and treat technologies [National Research Council (NRC), 1994]. Increasing attention has therefore been given to the evaluation of alternative remediation technologies and assessment of the benefits of partial mass removal for such DNAPL source zones [Saenton and Illangasekare, 2003; Stroo *et al.*, 2003].

[3] Possible benefits of DNAPL source zone mass reduction include decreased risk (receptor concentration or DNAPL mobility reduction), abbreviated source longevity, reduced site management resource allocations, and enhancement of the potential for natural attenuation [Sale and McWhorter, 2001; Rao *et al.*, 2002]. Risk to human health can be quantified in terms of groundwater contaminant

concentrations relative to a concentration threshold (e.g., maximum contaminant level, MCL) [Freeze and McWhorter, 1997], contaminant mass within the plume [Feenstra et al., 1996], or contaminant flux across a control plane at a downgradient point of compliance [Einarson and Mackay, 2001]. Risk reduction associated with cleanup of DNAPL source zones can therefore be measured in terms of (1) decreasing contaminant concentrations at downstream receptors, (2) decreasing contaminant plume mass, or (3) decreasing contaminant flux at successive downgradient control planes [Rao et al., 2002]. Ultimately, however, predictions of downgradient aqueous phase contaminant concentrations and mass flux depend on the initial and evolving configurations of pools and entrapped residual NAPL in the source zones.

[4] Conceptual models describing the distribution of DNAPL within source zones have been articulated by Kueper and Frind [1991b], Anderson et al. [1992], Feenstra et al. [1996], and Sale and McWhorter [2001]. Such conceptualizations are based on observations of DNAPL distributions in laboratory experiments [Kueper et al., 1989; Rathfelder et al., 2003], field settings [Poulsen and Kueper, 1992; Kueper et al., 1993], and numerical simulations in spatially variable porous media [Kueper and Frind, 1991b; Kueper and Gerhard, 1995; Dekker and Abriola, 2000a]. In these investigations, DNAPL source zones are characterized by contaminated regions of irregular saturation distributions and complex boundaries. In stratified porous media, a relatively small degree of horizontal bedding has been observed to result in a pronounced preferential lateral migration of organic [Poulsen and Kueper, 1992; Essaid et al., 1993; Kueper et al., 1993]. DNAPL distributions in stratified media may be dominated by vertical fingers at residual saturation and thin horizontal lenses at higher saturations [Anderson et al., 1992]. Sale and McWhorter [2001] used the term “source-zone architecture” to refer collectively to the distribution (i.e., size, shape, location, and saturation) of DNAPL subzones comprising an overall DNAPL source zone.

[5] Attempts to evaluate the influence of source zone architecture on DNAPL dissolution phenomena and dissolved mass flux have led to mixed conclusions, with results highly dependent upon the conceptual model employed. Investigations using analytical solutions for simple, deterministically shaped geometries (i.e., rectangles, ellipses, or spheres) of ganglia and pools embedded within uniform flow fields have suggested that groundwater extraction would be ineffective at removing NAPL contaminant within a reasonable time period and that removal of most of the DNAPL mass would be required before dissolved contaminant concentrations would be reduced below regulatory limits [Hunt et al., 1988; Chrysikopoulos, 1995; Sale and McWhorter, 2001]. Alternatively, an analysis employing uniform NAPL distributions within stream tubes characterized by a lognormal velocity distribution estimated contaminant mass flux reductions of more than 80% after removal of less than half of the DNAPL mass [Rao and Jawitz, 2003]. Numerical analysis of mass flux assuming nonuniform DNAPL distributions within a nonuniform flow field predicted enhanced contaminant mass flux reduction when NAPL saturation was negatively correlated with hydraulic conductivity [Rao et al., 2002].

[6] The divergence of conclusions regarding the benefits of partial DNAPL source zone mass removal based on models incorporating idealized descriptions of organic liquid distribution suggests the need to explore more realistic representations of spatially variable organic entrapment within DNAPL source zones. Models simulating the establishment of DNAPL source zones must be able to reproduce organic liquid spreading, fingering, and pooling, characteristic of DNAPL source zone architecture in real settings [Strategic Environmental Research and Development Program and Environmental Security Technology Certification Program, 2002]. Models simulating the remediation of DNAPL source zones must incorporate the dependence of entrapped DNAPL dissolution dynamics and mass transfer rates upon flow velocities [e.g., Powers et al., 1991, 1992]. In addition, models should account for preferential flow paths and low-permeability zones that can influence the delivery of flushing fluids and subsequent advective transport of solubilized or mobilized contaminant [Fountain et al., 1996; Fountain, 1997; Saenton et al., 2002]. Consequently, numerical multiphase, multicomponent flow and transport simulators, capable of incorporating rate-limited mass transfer and spatial variability in aquifer properties, provide an important means to predict dissolved phase contaminant flux and to evaluate potential benefits of partial mass removal from DNAPL source zones in nonuniform flow fields.

[7] This paper describes a numerical investigation of the influence of hydraulic property correlation on DNAPL source zone architecture and the relationship among DNAPL architecture, organic liquid recovery by surfactant solubilization, and resultant aqueous phase mass flux in a statistically homogeneous, nonuniform sand aquifer. Geostatistical models characterizing the spatial variability of the aquifer provided the means to generate multiple realizations of organic liquid saturation distributions resulting from a hypothetical tetrachloroethylene (PCE) spill [Lemke et al., 2004]. Resulting PCE distributions are incorporated as initial conditions for the analysis of DNAPL recovery in nonuniform velocity fields using a laboratory-validated multiphase, multicomponent transport simulator accounting for rate-limited mass transfer. Source zone architecture is quantified in terms of model cells classified as “pool” or “ganglia” zones on the basis of the initial DNAPL saturation. The relation of source zone architecture to the spatial distribution of aquifer properties and the evolution of source zone architecture in response to partial DNAPL mass removal are examined. Further inferences are then drawn regarding decreases in dissolved contaminant mass flux in response to partial DNAPL source zone mass removal.

2. Methods

2.1. Aquifer Characterization and Variability Modeling

[8] The aquifer chosen to provide a basis for alternative characterization models used in this study is located in Oscoda, Michigan, USA, at the site of a former dry cleaning business. A suspected DNAPL source zone was identified beneath the building in an unconfined aquifer composed of relatively homogeneous glacial outwash sands and underlain by a thick clay layer approximately 8 m below the

Table 1. Variable Treatment of Intrinsic Permeability, Porosity, and Brooks-Corey Capillary Pressure-Saturation Parameters Among the Four Alternative Simulation Sets Constructed by Lemke et al. [2004]

	Reference Set (Conventional)	Simulation Set 1	Simulation Set 2	Simulation Set 3
Porosity ϕ	uniform	uniform	variable (SGS)	variable (SGS)
Permeability k	SGS	SIS $k = f(d_{10})$	SIS $k = f(d_{10}, \phi)$	SIS $k = f(d_{10}, \phi)$
Brooks-Corey P_c -Sat	uniform λ , scaling of single P_b	uniform λ , scaling of single P_b	uniform λ , scaling of single P_b	HPM: $\lambda, P_b = f(\text{SIS class}, \phi)$
Leverett scaling	$P_b = f(\sqrt{k})$	$P_b = f(\sqrt{k})$	$P_b = f(\sqrt{k} = f(d_{10}, \phi))$	none

ground surface. In the summer of 2000, a pilot-scale surfactant-enhanced aquifer remediation (SEAR) test was conducted at the site to solubilize and recover PCE from the suspected DNAPL source zone under the building [Abriola et al., 2001]. A 4% (weight) polyoxyethylene (20) sorbitan monooleate (Tween 80) surfactant formulation was selected based upon a demonstrated capacity to solubilize PCE [Pennell et al., 1997] without remobilization due to lowering of the NAPL-water interfacial tension [Ramsburg and Pennell, 2001]. Detailed descriptions of the test design are provided by Drummond et al. [2000] and L. M. Abriola et al. (A pilot-scale demonstration of surfactant-enhanced PCE solubilization at the Bachman Road site: (1) Site characterization and test design, submitted to *Environmental Science and Technology*, 2004). The spatial distribution of aquifer properties and the magnitude of hydraulic gradients utilized in this investigation are representative of, but not meant to explicitly reproduce, the conditions found at the field site.

[9] Site characterization data were collected from continuous core samples containing relatively homogeneous fine- to medium-grained sand [Lemke et al., 2004]. The arithmetic mean porosity in 162 repacked samples was 0.36. Hydraulic conductivity, K , values measured in ten repacked samples and estimated from 167 grain size distributions were nonuniform, ranging from 1 to 48 m/d. Variance of the lognormal transformation of the estimated K values ($\sigma^2 \ln(K)$) was 0.29.

[10] Constitutive relationships describing fluid retention, relative permeability, hysteresis, and entrapment were represented with common parameterizations. Capillary pressure-saturation (P_c -Sat) relationships were modeled using a Brooks and Corey [1964] formulation:

$$\bar{S}_w = \frac{S_w - S_{wr}}{1 - S_{wr}} = \left(\frac{P_b}{P_c} \right)^\lambda \quad P_c \geq P_b; \quad (1)$$

$$\bar{S}_w = 1.0 \quad P_c < P_b, \quad (2)$$

where S_w is the wetting phase saturation, \bar{S}_w is the effective wetting phase saturation, S_{wr} is the residual or irreducible

wetting phase saturation, P_b is the entry pressure, and λ is the pore size distribution factor. P_b and λ values, estimated directly from grain size distribution curves and porosity values using the Haverkamp and Parlange [1986] method, were validated with air-water laboratory measurements in eight representative samples [Lemke et al., 2004]. The Brooks and Corey [1964] extension of the Burdine [1953] model was employed to define a relative permeability function. Hysteresis due to nonwetting phase entrapment was incorporated through the inclusion of apparent water saturations and the quantity of entrapped organic phase was estimated using the method of Parker and Lenhard [1987].

[11] Spatial variability in aquifer properties and constitutive parameters was modeled using four alternative approaches described by Lemke et al. [2004] (Table 1). These approaches utilized sequential Gaussian simulation (SGS) and sequential indicator simulation (SIS) [Deutsch and Journel, 1998] to generate three-dimensional conditioned porosity, ϕ , and permeability, k , fields. Representative P_c -Sat parameters were either scaled to the ϕ and k fields using Leverett [1941] scaling (reference set and sets 1 and 2), or estimated independently using the Haverkamp and Parlange [1986] method applied to weighted grain size distributions corresponding to the simulated indicator class at each grid node (set 3). Ensembles employing Leverett scaling resulted in perfectly correlated P_b and k fields, whereas the Haverkamp and Parlange approach led to variable λ and P_b values that were strongly associated with the spatial distribution of indicator classes. Ensemble mean parameter values and correlation coefficients for simulation sets 2 and 3 are given in Table 2. In all cases, estimated air-water P_c values were scaled to the PCE-water system using a ratio of interfacial tensions, consistent with the experimental results of Demond and Roberts [1991] for the behavior of quartz sand systems with organic liquid-water interfacial tensions greater than 30 dyn/cm.

2.2. PCE Infiltration and Entrapment Modeling

[12] PCE infiltration was simulated with the immiscible fluid flow model, MVALOR [Abriola et al., 1992;

Table 2. Ensemble Arithmetic Mean, Variance, and Bivariate Correlation Coefficients for Aquifer Parameters^a

	Mean	Variance	ϕ	$\ln(K)$	$\ln(P_b)$	λ	S_o
Mean			0.363	-3.88	7.73	2.44	0.019
Variance			2.4E-4	0.212	0.041	0.095	0.010
ϕ	0.363	2.4E-4	-	0.372	0.629	-0.702	-0.152
$\ln(K)$	-3.88	0.212	0.372	-	-0.255	-0.360	-0.039
$\ln(P_b)$	7.84	0.050	-0.285	-0.996	-	-0.520	-0.177
λ	2.08	0.000	0.000	0.000	0.000	-	0.118
S_o	0.017	0.001	0.033	0.089	-0.089	0.000	-

^aValues below the diagonal correspond to correlated simulation set 2. Values above the diagonal correspond to independent simulation set 3. K is in cm/s; P_b is in Pa. Read 2.4E-4 as 2.4×10^{-4} .

Table 3. DNAPL Source Zone Characterization Metrics for MVALOR PCE Infiltration and Entrapment Simulations Conducted by Lemke et al. [2004]^a

	Metric Value				Associated Realization Number		
	Minimum	Mean	Maximum	SD ^b	Minimum	Mean	Maximum
Reference set							
S_o max ^c	0.172	0.355	0.625	0.086	13	36	23
σ_{xx}^2 ^d	0.273	0.663	1.722	0.295	41	27	44
σ_{zz}^2 ^e	2.193	4.418	7.856	1.367	49	2	17
Set 1							
S_o max	0.210	0.358	0.501	0.080	3	11	32
σ_{xx}^2	0.263	0.530	2.177	0.284	18	40	17
σ_{zz}^2	2.459	4.117	6.112	0.909	17	3	1
Set 2							
S_o max	0.198	0.370	0.567	0.086	20	49	36
σ_{xx}^2	0.227	0.545	2.550	0.320	36	35	17
σ_{zz}^2	2.417	4.157	7.476	0.971	17	14	36
Set 3							
S_o max	0.900	0.910	0.915	0.004	13	28	7
σ_{xx}^2	0.174	0.433	0.868	0.166	7	47	11
σ_{zz}^2	0.648	4.202	9.551	2.311	12	43	18

^aData are reported for 50 realizations in each simulation set.

^bSD is standard deviation.

^c S_o max is maximum organic saturation at end of DNAPL redistribution period.

^dHere σ_{xx}^2 is second spatial moment about X center of mass.

^eHere σ_{zz}^2 is second spatial moment about Z center of mass.

Rathfelder and Abriola, 1998], using 7.9×9.8 m two-dimensional profiles extracted from each three-dimensional geostatistical realization. A unit width of 1.0 m was used for the third dimension to accommodate volumetric and saturation calculations. The profile position and orientation were chosen to correspond to a flow path between a surfactant injection well and the SEAR test extraction well. Horizontal and vertical grid discretization was 30.48 and 7.62 cm, respectively, (26 columns \times 128 rows). Horizontal and vertical ranges, determined from experimental k semivariograms fit with a spherical semivariogram model, were 700 and 107 cm, respectively. In the simulated spill, 96 L (156 kg) of PCE was released over four grid cells at the top center of the model domain, which was assumed to correspond to the water table. An ensemble of 50 realizations was simulated from each set of alternative aquifer models. Similarities and differences in DNAPL entrapment behavior predicted by MVALOR were quantified for each ensemble using a set of metrics including spatial moments and PCE saturations (Table 3). A complete description of the PCE spill modeling effort is given by Lemke et al. [2004].

[13] The largest differences among PCE distributions were observed between ensembles that did (reference set, sets 1 and 2) or did not (set 3) employ Leverett scaling, even when ensembles shared identical ϕ and k distributions. Simulations from ensemble set 3, which used the Haverkamp and Parlange [1986] method to assign capillary parameters, exhibited increased infiltration, decreased spreading, and an increased tendency for DNAPL pooling, reflected in maximum organic saturations exceeding 0.60 [Lemke et al., 2004]. These differences in DNAPL distributions manifest themselves in dissimilar DNAPL source zone architectures as quantified and discussed

below. On the basis of their use of Leverett scaling, the reference and simulation sets 1 and 2 are herein referred to collectively as correlated ensembles, while realizations comprising simulation set 3 are referred to as independent realizations.

2.3. DNAPL Recovery Modeling

[14] MVALOR PCE saturation distributions were used as initial conditions for the simulation of organic recovery under SEAR using MISER [Abriola et al., 1997; Rathfelder et al., 2000], a two-dimensional compositional simulator that accounts for rate-limited NAPL dissolution and surfactant sorption. In MISER, fluid flow is described with a general balance equation for phase α , which may be composed of multiple components, i :

$$\frac{\partial}{\partial t}(\rho_\alpha \phi S_\alpha) - \nabla \cdot \left(\rho_\alpha \frac{\mathbf{k} k_{r\alpha}}{\mu_\alpha} (\nabla P_\alpha - \rho_\alpha \mathbf{g}) \right) = \sum_i I_\alpha^i + \sum_i \Gamma_\alpha^i \quad (3)$$

where ρ_α is the intrinsic mass density of phase α ; ϕ is the matrix porosity; S_α is the saturation of phase α ; \mathbf{k} is the intrinsic permeability tensor of the medium; $k_{r\alpha}$ is the relative permeability of the α phase; μ_α is the α phase dynamic viscosity; P_α is the fluid phase thermodynamic pressure; \mathbf{g} is the gravity vector; I_α^i is the source/sink of component i in the α phase due to phase mass exchange processes such as volatilization, dissolution and sorption; and Γ_α^i is the external supply of species i to the α phase due to intraphase compositional transformations. For the MISER simulations described here, the aqueous phase was treated as mobile but NAPL was considered to be entrapped and therefore immobile. Mobilization of entrapped organic liquid in response to interfacial tension reduction associated with the application of surfactant was not permitted.

[15] A second system of equations is used to describe the conservation of mass of individual chemical components within each phase. The general form of these equations is given as:

$$\begin{aligned} \frac{\partial}{\partial t}(\rho_\alpha \phi S_\alpha \omega_\alpha^i) - \nabla \cdot (\rho_\alpha \phi S_\alpha \omega_\alpha^i \mathbf{v}_\alpha) - \nabla \cdot (\rho_\alpha \phi S_\alpha \mathbf{D}_\alpha^i \cdot \nabla \omega_\alpha^i) \\ = I_\alpha^i + \Gamma_\alpha^i. \end{aligned} \quad (4)$$

Here ω_α^i is the mass fraction of component i in phase α ; \mathbf{D}_α^i is the hydrodynamic dispersion tensor; and \mathbf{v}_α is the average pore velocity of the α phase. Nonequilibrium interphase mass exchange between α and β phases is modeled with a linear driving force expression [Weber and DiGiano, 1996]:

$$I_\alpha^i = \hat{k}_{\alpha\beta}^i (\omega_{\alpha e}^i - \omega_\alpha^i) \quad (5)$$

where $\omega_{\alpha e}^i$ is the mass fraction of component i , which is in equilibrium with the mass fraction of i in the β phase and $\hat{k}_{\alpha\beta}^i$ is a lumped mass exchange coefficient. Equation (5) is used to describe all interphase mass transfer couplings. For fluid-fluid partitioning, equilibrium mass fraction values are determined from Raoult's and Henry's laws or laboratory-measured equilibrium solubilization relations. Lumped mass exchange coefficients are expressed as functions of media and fluid properties such as pore velocity, saturation, and pore structure [e.g., Powers et al., 1992, 1994]. The effect of composition on liquid phase density is

Table 4. Soil Properties Used in Simulations

Soil Characteristics	Value
Median grain size d_{50} , μm	295
Uniformity index	1.86
K_v/K_h anisotropy ratio	0.5
Bulk soil density, g/cm^3	1.75
Soil organic fraction	0.001
Longitudinal dispersivity α_L , m	0.30
Transverse dispersivity α_T , m	0.0075
PCE-water retention characteristics	
Residual water saturation S_{wr}	0.071
Residual organic saturation S_{or}	0.151
Brooks-Corey entry pressure P_b , Pa	1400–8700
Brooks-Corey pore size distribution factor λ	1.4–3.6
Air-water interfacial tension, dyn/cm	72.0
PCE-water interfacial tension, dyn/cm	47.8
Surfactant sorption parameters	
Langmuir limiting sorption capacity Q_{ms} , mg/g	0.165
Langmuir b_s , L/mg	0.118
PCE sorption parameters	
Linear sorption coefficient K_d , cm^3/g	0.17

incorporated through Amagat's Law. For aqueous-solid partitioning, nonlinear sorption isotherms are employed to determine equilibrium concentrations. MISER has been verified against analytical solutions and numerical models [Abriola *et al.*, 1997], as well as laboratory column and sandbox experiments, [e.g., Rathfelder *et al.*, 2001; Taylor *et al.*, 2004].

[16] For the MISER simulations described herein, constant pressure boundary conditions were applied to simulate PCE dissolution under natural aqueous gradient (0.002) conditions for a period of 100 days. This period was sufficient to pass slightly more than one pore volume of water through the model domain and stabilize PCE concentrations at the effluent boundary. Next, SEAR was simulated at a higher gradient (0.130) for 2 days, followed by a water flood at the same gradient for 10 days. The 0.130 gradient, chosen for consistency with predicted gradients along flow paths connecting surfactant injection and extraction wells in three-dimensional simulations of the SEAR pilot test, was judged to be representative of potential field conditions. Simulated SEAR involved the injection of approximately 1.6 pore volumes of 4% Tween 80 aqueous surfactant solution. At equilibrium, the PCE solubilization capacity of 4% Tween 80 is approximately 26,880 mg/L [Taylor *et al.*, 2001]. Subsequent water flooding, to recover injected surfactant,

involved approximately 8.0 additional pore volumes. Finally, natural gradient flow was resumed for 100 days. This approach allows pre- and post-SEAR PCE effluent concentrations to be compared under natural gradient conditions.

[17] MISER simulation parameters are listed in Tables 4 and 5. Simulations modeled rate-limited PCE solubilization using two mass transfer correlations, that of Powers *et al.* [1992] for aqueous dissolution and that of Taylor *et al.* [2001], following the approach of Rathfelder *et al.* [2001], when surfactant concentrations exceeded the critical micelle concentration. The Powers *et al.* [1992] correlation employed a single NAPL sphere class with a radius of 0.2 mm. A longitudinal dispersivity value of 0.3 m was estimated based on breakthrough history matching in three-dimensional solute transport models of alcohol tracer tests conducted at the site [Abriola *et al.*, 2001]. For the 2-day SEAR scenario evaluated, PCE recovery and aqueous phase mass flux estimates were found to be insensitive to transverse dispersivity values ranging from 0.0075 to 0.06 m, so the smallest value of 0.0075 m was adopted. Smaller values led to convergence problems in MISER simulations for some realizations. Organic sorption was neglected after laboratory-measured linear, equilibrium PCE sorption and coupled Langmuir surfactant sorption [Pennell *et al.*, 2002] were determined to have a limited influence on PCE recovery and post-SEAR PCE effluent concentrations. This observation is in accordance with results of Taylor *et al.* [2001] who found that surfactant sorption had little effect on subsurface surfactant transport in systems with relatively small Langmuir limiting sorption capacity, Q_{ms} , values. The first set of numerical PCE dissolution experiments was run on a group of Sun Microsystems Ultra 1, Ultra 5, and Ultra 10 workstations. The average CPU time for each of the initial 200 simulations was 2.5 hours.

[18] A second series of simulations was conducted to explore differences in the evolution of source zone architecture and the resultant effluent mass flux as a function of the extent of DNAPL recovery. Representative realizations spanning the range of predicted infiltration and entrapment behavior were selected from each of the four alternative stochastic simulation sets on the basis of minimum, mean, and maximum organic liquid spreading and saturation metrics (Table 3). The duration of the surfactant injection period was varied to generate a series of mass flux estimates associated with modeled remediation efficiencies ranging from 0 to 99% DNAPL recovery. Ten to twelve

Table 5. Fluid Properties Used in Simulations

	Water	PCE	Tween 80
Temperature, $^{\circ}\text{C}$	15	15	15
Molecular weight, g/mol	18.0	165.80 ^a	1310.0 ^a
Liquid density, g/mL	0.9990	1.6230 ^a	1.0700 ^a
Weight solubilization ratio, g/g	–	–	0.589 ^{a,b}
Aqueous diffusivity, cm^2/s	–	8.6×10^{-6c}	1.48×10^{-6c}
Critical micelle concentration, mg/L	–	–	35.0 ^d
Aqueous solubility, g/L	–	0.1489 ^e	–

^aSee Taylor *et al.* [2001].

^bSee Pennell *et al.* [1997].

^cSee Dekker and Abriola [2000b].

^dSee Yeh *et al.* [1999].

^eSee Horvath [1982].

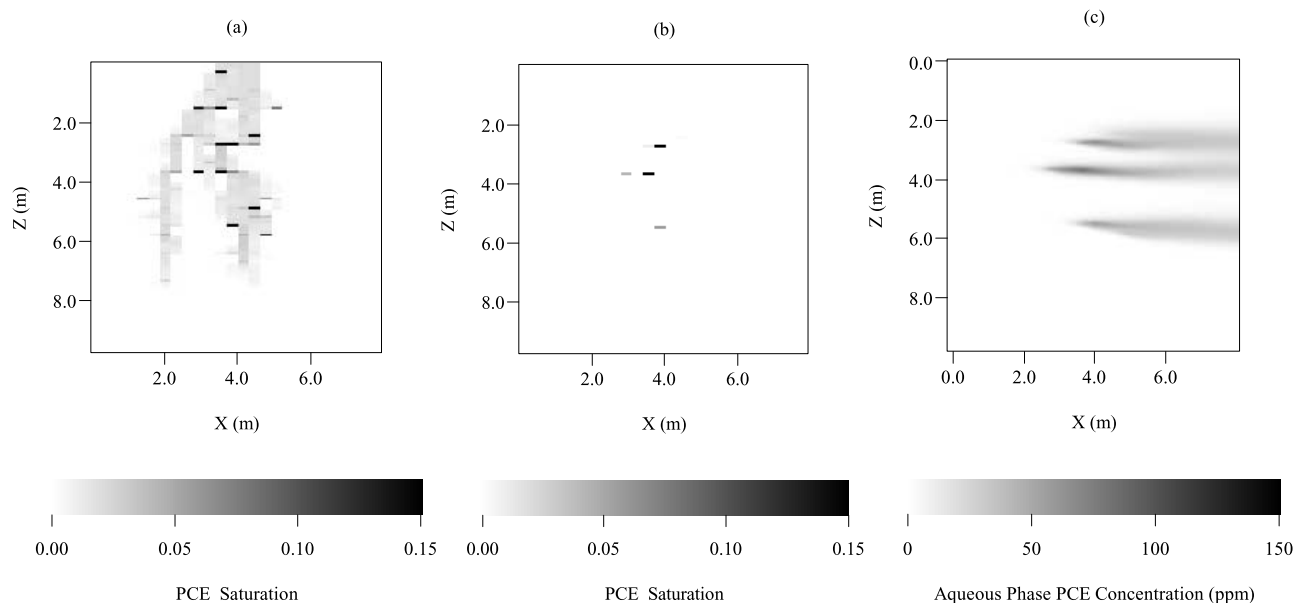


Figure 1. NAPL source zone architecture and dissolved PCE concentrations for realization number 49 from correlated set 2: (a) pre-SEAR PCE saturations, (b) post-SEAR PCE saturations (95.6% PCE recovery), and (c) post-SEAR PCE concentrations under natural gradient conditions (maximum predicted cell concentration is 85 ppm). Flow is from left to right. See color version of this figure in the HTML.

different surfactant injection periods were used for each realization evaluated, necessitating 620 runs for this series of simulations.

[19] A final series of simulations was performed to investigate the evolution of source zone architecture in response to long-term dissolution of DNAPL under natural gradient conditions. These simulations were run using a 0.001 gradient for a period of twenty years. Representative realizations from simulation sets 2 and 3 with minimum, mean, and maximum organic liquid spreading and saturation metrics (Table 3) were included.

3. Results

3.1. Pre-SEAR DNAPL Source Zone Architecture

[20] The initial distribution of entrapped DNAPL in each realization was analyzed to characterize variability in initial DNAPL source zone architecture. As a working approach, regions of the model domain with organic liquid saturations exceeding the maximum residual organic saturation ($S_{or} = 0.151$) were classified as pools while those containing organic liquid saturations at or below S_{or} were classified as ganglia. Cells with organic liquid saturations below the numerical convergence criterion of 0.0001 were treated as NAPL free. Pre-SEAR PCE saturations for representative realizations from sets 2 and 3 are depicted in Figures 1a and 2a, respectively. For plotting purposes the maximum value of the gray scale was set to 15.1% to highlight DNAPL source zone architecture defined by the distribution of model elements classified as pools or ganglia. Note that pooled PCE at saturations in excess of residual occurs in individual cells due to the absence of a driving force sufficient to overcome contrasts in capillary entry pressures across adjacent cell boundaries. Organic liquid saturations in such cells were stable at the end of the simulated redistribution period. The percentage of PCE

mass residing in pools (cells exceeding S_{or}) was also calculated for each ensemble (Table 6). Prior to SEAR simulation, realizations from correlated ensembles initially contained a relatively small NAPL fraction within pools (3% to 45%) and a commensurately large ganglia NAPL fraction. In contrast, independent realizations initially contained a higher percentage of pooled DNAPL (28% to 85%).

[21] Configurations of pool and ganglia elements were examined with respect to their distribution in the vertical and horizontal directions. The vertical distribution of pool and ganglia elements was quantified by the number of model rows (from 0 to 128) containing at least one cell of the respective classification. Similarly, the horizontal distribution was quantified using the number of columns (0 to 26). Results for pool and ganglia elements are presented in Table 7. Mean counts of rows and columns containing pool elements are larger for the independent ensemble, which contained proportionately more mass in cells with high organic saturations. Mean row and column ganglia element counts are generally similar for correlated and independent ensembles, suggesting that initial overall DNAPL source zone dimensions were similar among ensemble sets. A more rigorous analysis of the spatial distribution of PCE saturations treated as a continuous variable using metrics defined on the basis of spatial moments is given by Lemke *et al.* [2004]. However, for the purposes of relating DNAPL source zone architecture to the formation of contaminant plumes, cell counts provide a potentially useful means of determining the contribution of spreading phenomena to prerediation mass flux or the role of persistence phenomena in controlling postremediation mass flux.

[22] The correspondence of initial PCE saturation distributions to aquifer properties within coincident model cells was also examined to evaluate the extent of correlation

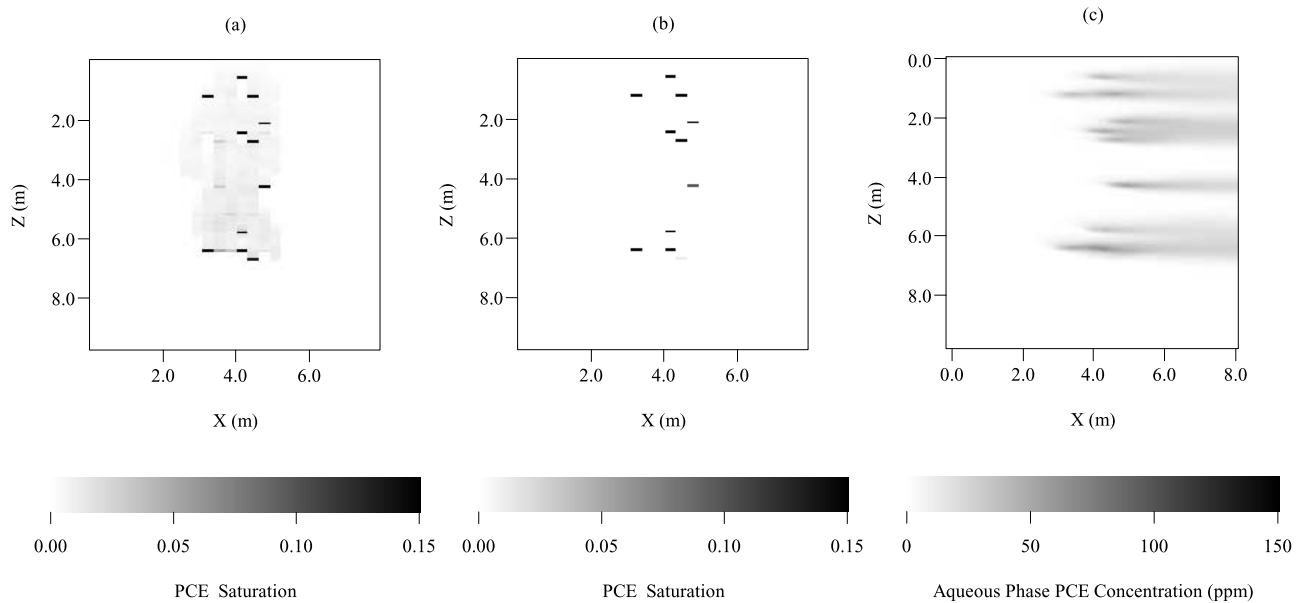


Figure 2. NAPL source zone architecture and dissolved PCE concentrations for realization number 28 from independent set 3: (a) pre-SEAR PCE saturations, (b) post-SEAR PCE saturations (57.9% PCE recovery), and (c) post-SEAR PCE concentrations under natural gradient conditions (maximum predicted cell concentration is 60 ppm). Flow is from left to right. See color version of this figure in the HTML.

between organic liquid saturation and permeability that has been postulated by others [e.g., *Anderson et al.*, 1992; *Berglund*, 1997; *Rao et al.*, 2002]. Plots of S_o versus K in model cells presented in Figure 3 do not support such correlations for nonuniform aquifers, whether or not Leverett scaling is employed. Figure 3a includes data for all cells containing PCE in 50 realizations from correlated set 2. Data points for cells containing PCE in 50 realizations from independent set 3 are included in Figure 3b. Note that realizations in sets 2 and 3 contain equivalent ϕ and K distributions (Table 1). Correlation coefficients between collocated S_o and $\ln(K)$ values are less than 0.1 for both ensembles (Table 2). Direct correlations between organic liquid saturation and capillary entry pressure are also unsupported (Figure 4). Although higher saturations are present in the independent ensemble, no discernable correlation between S_o and K or P_b is evident in these plots.

[23] Plots of S_o versus vertical K contrast and S_o versus vertical P_b contrast for the same ensembles are presented in Figures 5 and 6, respectively. Here, the vertical contrast in K and P_b is defined as the signed difference between values in vertically adjacent cells (overlying cell minus the underlying cell). In correlated realizations, organic liquid

saturations exceeding 0.05 are present only in cells with positive K contrast (Figure 5a) and negative P_b contrast (Figure 6a). The symmetry of Figures 5a and 6a reflect the spatial dependence of K and P_b values imposed through Leverett scaling. When scaling is employed, K contrast can effectively serve as a surrogate for entry pressure contrast. No clear relationship can be seen between S_o and vertical K contrast in independent realizations (Figure 5b). Correlations between S_o and vertical P_b contrast (Figure 6), however, do reveal that high organic liquid saturations are restricted to cells positioned above cells with higher entry pressures in both correlated and independent realizations. Therefore entry pressure contrast is a more general determinant of pooling (i.e., high organic liquid saturation) than K contrast. Nevertheless, Figure 6 contains a large amount of scatter, reflecting the path-dependent nature of organic liquid saturation accumulating in model cells following a simulated DNAPL spill. A small number of cells exhibit higher saturations where no vertical K or P_b contrast exists. This indicates DNAPL pooling in vertically adjacent cells with the same K and P_b values. Vertical arrangement of cells with identical properties resulted from the discretization scheme which divided aquifer property blocks originally simulated at a 30.5 cm increment into finer

Table 6. DNAPL Mass Fraction Contained in Pools^a

	Pre-SEAR				Post-SEAR			
	Minimum	Mean	Maximum	SD	Minimum	Mean	Maximum	SD
Reference set	0.029	0.158	0.454	0.077	0.000	0.946	1.00	0.056
Set 1	0.047	0.144	0.304	0.059	0.834	0.987	1.00	0.031
Set 2	0.066	0.161	0.340	0.062	0.000	0.969	1.00	0.026
Set 3	0.280	0.585	0.853	0.136	0.989	0.999	1.00	0.003

^aInitial conditions (pre-SEAR) and 2-day SEAR simulation results are reported for 50 realizations in each simulation set.

Table 7. Pre-SEAR Distribution of Cells Originally Classified as Pool or Ganglia^a

	Pool						Ganglia					
	Vertical			Horizontal			Vertical			Horizontal		
	Minimum	Mean	Maximum	Minimum	Mean	Maximum	Minimum	Mean	Maximum	Minimum	Mean	Maximum
Reference set	2	5.3	13	2	5.8	10	80	110.5	128	12	14.7	19
Set 1	2	4.6	8	1	4.9	9	72	110.7	128	10	13.8	18
Set 2	2	5.0	12	2	5.2	8	72	109.6	128	11	14.0	19
Set 3	2	5.8	12	2	6.2	10	60	107.2	128	10	12.9	19

^aReported values represent the number of rows (vertical distribution, maximum = 128) or columns (horizontal distribution, maximum = 26) containing at least one cell classified as a pool or ganglia element. Fifty realizations were analyzed for each simulation set.

7.6 cm increments needed to better resolve capillary effects [Lemke *et al.*, 2004].

3.2. Post-SEAR DNAPL Source Zone Architecture

[24] The presence of persistent PCE in the form of pool and ganglia elements following simulated SEAR is visible in Figures 1b and 2b, which show representative DNAPL realizations from sets 2 and 3 respectively. Following the simulated 2-day surfactant flush, most realizations from all simulation sets were dominated by saturations attributable to cells originally classified as pools (Table 6). However, PCE in zones originally classified as ganglia persisted following SEAR simulation in approximately 45% of the realizations. Two conditions were found to result in the persistence of such ganglia cells. Dissolution of organic liquid from upgradient pools led to aqueous phase PCE concentrations approaching the solubility limit, thus reducing the driving force for dissolution in downgradient ganglia cells. Alternatively, sheltering from high-velocity flow by contiguous cells with low K values inhibited mass transfer from the NAPL to the aqueous phase. In two of the 200 realizations, PCE saturations in cells originally classified as ganglia persisted longer than pools following SEAR simulation.

[25] Continuing dissolution of PCE from persistent pool and ganglia cells under natural gradient flow is responsible

for post-SEAR aqueous phase contaminant mass flux. Both the magnitude and distribution of simulated dissolved phase contaminant flux are a function of the number and spatial arrangement of these cells. Post-SEAR vertical and horizontal pool and ganglia cell counts are presented in Table 8. Comparison with pre-SEAR values (Table 7) reveals that pool elements persist to a far greater degree than ganglia elements, in accordance with the observation that post-SEAR DNAPL mass is contained primarily within pools (Table 6). On average, pools occupy slightly more column and row positions in the independent ensemble. However, these differences are small in comparison to differences in DNAPL recovery between correlated and independent ensembles discussed below.

3.3. DNAPL Recovery and Mass Flux

[26] Table 9 summarizes predicted effluent PCE concentration and mass flux across the effluent boundary of the model domain following 100 days of groundwater flow and PCE dissolution simulated under natural gradient conditions in each ensemble set. Reported concentration values represent aqueous phase flux-weighted averages at 100 days, prior to the commencement of simulated SEAR. Similarities in ensemble mean cumulative pore volumes reflect similarities in the geometric mean hydraulic conductivity values among all ensemble sets. Similarities in

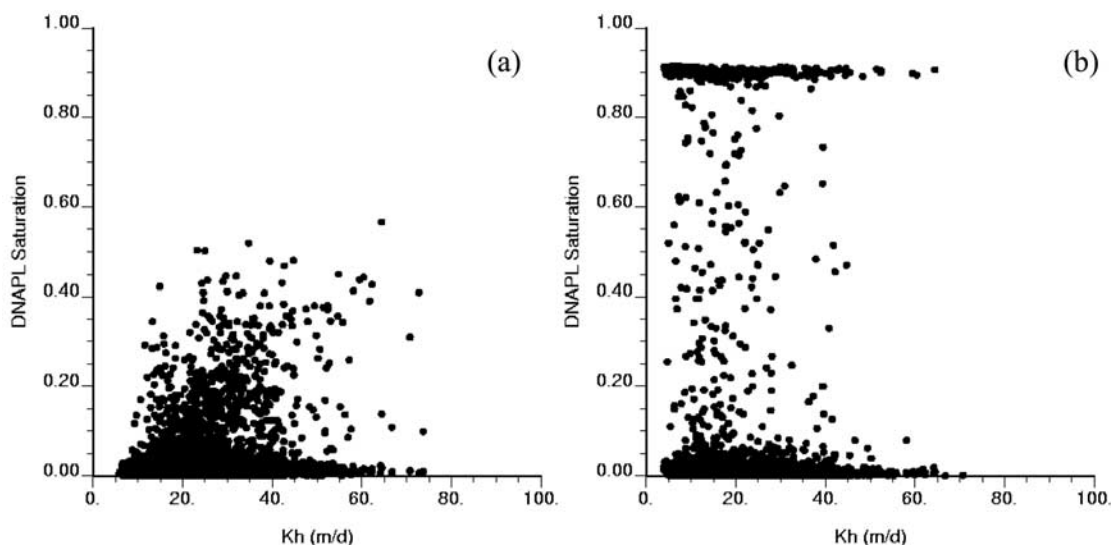


Figure 3. Organic liquid saturation, S_o , versus horizontal hydraulic conductivity, K_h : (a) cells containing PCE from 50 realizations in correlated set 2 ensemble and (b) cells containing PCE from 50 realizations in independent set 3 ensemble.

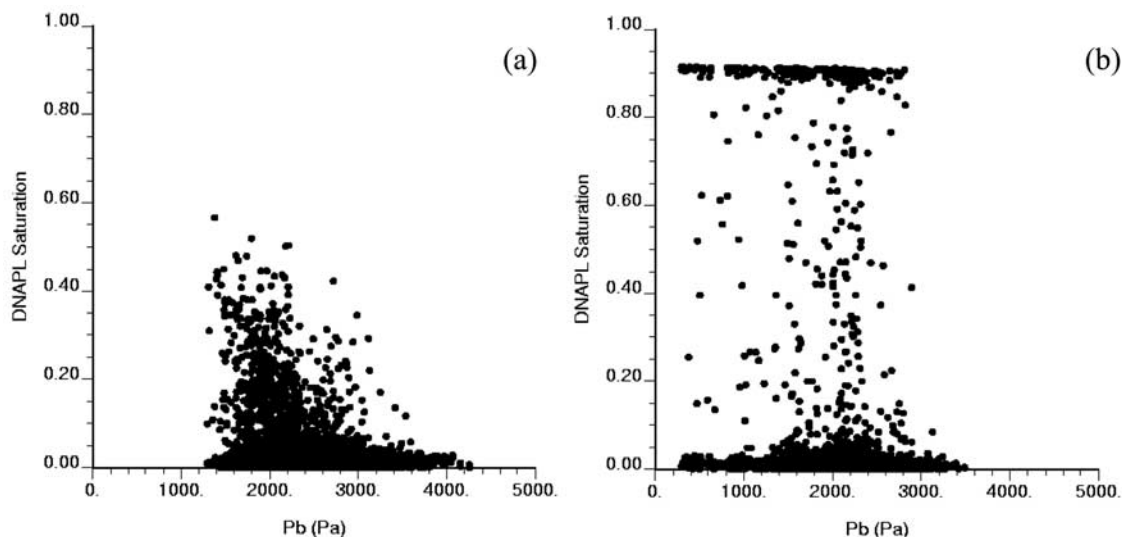


Figure 4. Organic liquid saturation, S_o , versus capillary entry pressure, P_b : (a) cells containing PCE from 50 realizations in correlated set 2 ensemble and (b) cells containing PCE from 50 realizations in independent set 3 ensemble.

ensemble mean effluent PCE concentration and mass flux values reflect similarities in the mean vertical distribution of cells containing organic liquid among ensembles (Table 7). The largest variability in initial concentration and mass flux occurs in the independent ensemble (set 3), reflecting a larger range in the vertical distribution of cells classified as ganglia (Table 7) as well as a larger variance in the fraction of DNAPL mass resident in pools (Table 6) in the independent ensemble set.

[27] Results for 2-day SEAR simulations for each ensemble set are presented in Table 10. PCE mass balance errors, normalized to mass initially in place, were less than 0.5%. Surfactant mass balance errors, normalized to injected mass flux, were less than 1.0%. Recall that aqueous phase PCE concentrations depicted in Figures 1c and 2c and reported in

Table 10 are calculated under natural gradient conditions. Simulated injection of approximately 1.6 pore volumes of surfactant solution resulted in the predicted removal of 28 to 100% of the PCE originally in place for the 200 realizations examined. Such recoveries are consistent with DNAPL mass removal observed in laboratory experiments. In two-dimensional sandbox experiments involving surfactant flushing of pooled and residual PCE from heterogeneous sand lenses, *Taylor et al.* [2001] recovered 70 to 81% of entrapped DNAPL using approximately 5 to 8 pore volumes of 4% Tween 80 solution. The overall initial PCE saturations for the sandbox experiments (1.0 to 3.5%) were higher than the organic liquid saturations averaged over the entire model domain in this investigation (0.35%), thus requiring more pore volumes of surfactant solution to

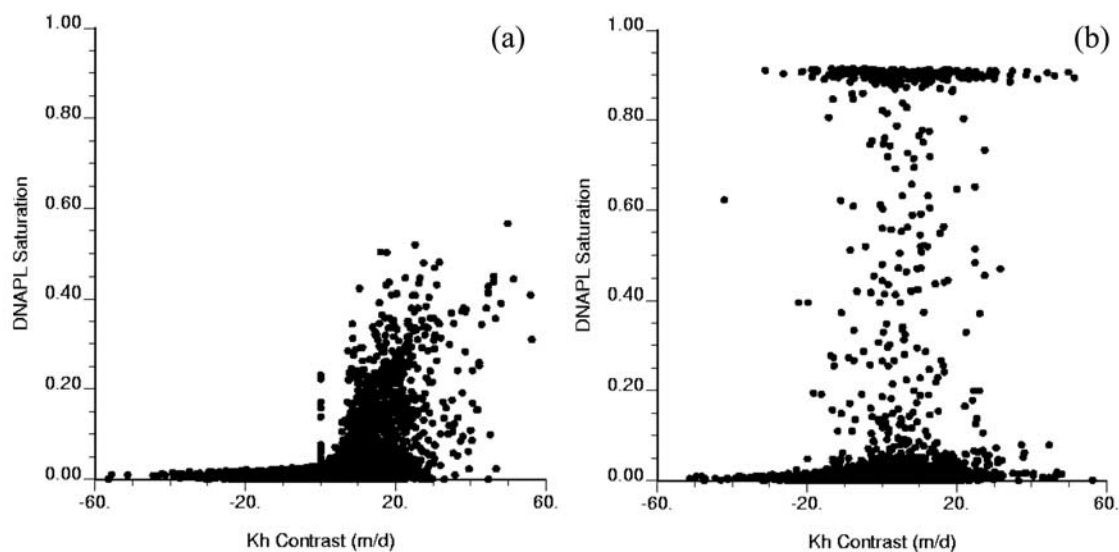


Figure 5. Organic liquid saturation, S_o , versus vertical K_h contrast: (a) cells containing PCE from 50 realizations in correlated set 2 ensemble and (b) cells containing PCE from 50 realizations in independent set 3 ensemble.

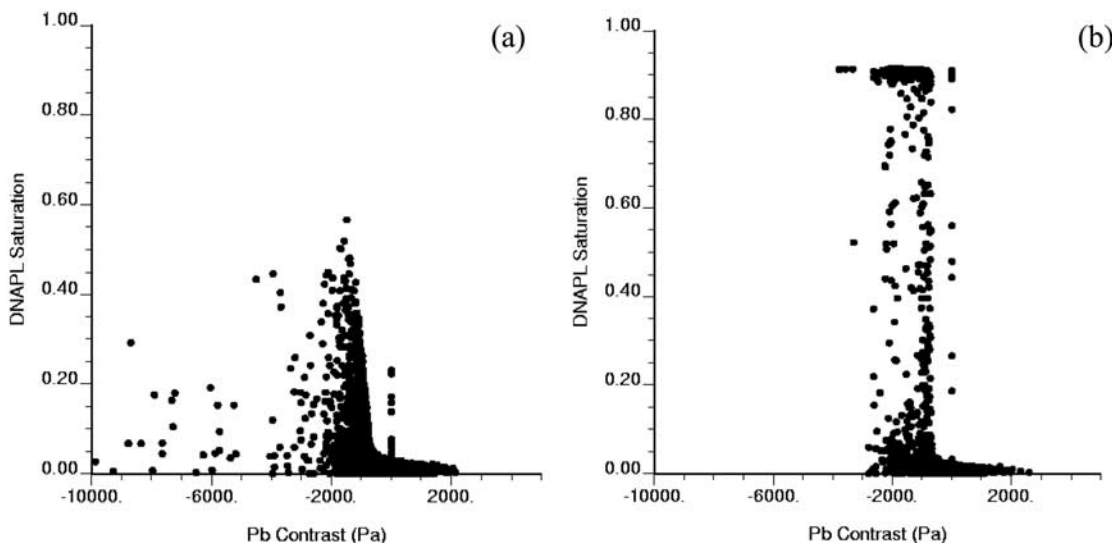


Figure 6. Organic liquid saturation, S_o , versus vertical P_b contrast: (a) cells containing PCE from 50 realizations in correlated set 2 ensemble and (b) cells containing PCE from 50 realizations in independent set 3 ensemble.

solubilize and recover similar fractions of NAPL originally in place.

[28] For the results reported herein, a notable contrast exists between the average PCE removal of 95 to 96% for the correlated ensembles and the mean removal of 57% for the independent ensemble, although simulated SEAR reduced concentrations by approximately two orders of magnitude relative to pre-SEAR conditions (Table 9) in all simulation sets. Remediation efficiency, measured in terms of mass removed per surfactant mass applied, is higher for the correlated ensembles. However, if measured in terms of the reduction of aqueous phase mass flux per PCE mass fraction removed, remediation efficiency is higher for the independent realizations.

[29] The evolution of source zone architecture and the resultant effluent mass flux as a function of the extent of DNAPL recovery was investigated in an additional series of simulations. Multiple simulation runs were conducted for each realization examined, varying the duration of the surfactant injection period from zero (i.e., water flood only) to 20 days to generate a series of mass flux estimates associated with DNAPL recoveries ranging from 0 to 99%. Because of the large computational demands required to evaluate the behavior of each realization, analysis was

initially limited to representative realizations selected from each of the four alternative stochastic simulation sets on the basis of minimum, mean, and maximum organic liquid spreading and saturation metrics (Table 3). Because of the greater variability observed in simulation results for representative independent realizations, all 50 realizations from set 3 were eventually included, however.

[30] Predicted contaminant mass flux as a function of PCE recovery in representative correlated realizations is presented in Figure 7. Flux-weighted PCE concentrations at the effluent model boundary are plotted as a function of percent PCE removed from the model domain. Such concentrations would be commensurate with measurements for a completely mixed sample taken in a fully screened observation well. Simulated concentrations reflect 100 days of postremediation flow under natural gradient flow conditions. Results for the 23 correlated realizations depicted in Figure 7 display similar patterns of effluent PCE concentration versus percent PCE removed. Greater than 60% DNAPL removal is required before PCE concentrations in the aqueous phase begin to fall appreciably. Removal of 65 to 90% DNAPL generally results in a one order of magnitude reduction in predicted effluent PCE concentrations.

Table 8. Post-SEAR Distribution of Cells Originally Classified as Pool or Ganglia^a

	Pool						Ganglia					
	Vertical			Horizontal			Vertical			Horizontal		
	Minimum	Mean	Maximum	Minimum	Mean	Maximum	Minimum	Mean	Maximum	Minimum	Mean	Maximum
Reference set	0	4.1	12	0	4.8	8	0	2.1	13	0	1.9	7
Set 1	1	3.7	7	1	4.3	8	0	0.7	4	0	0.7	5
Set 2	0	3.9	8	0	4.4	7	0	0.6	4	0	0.6	4
Set 3	0	5.4	9	0	6.0	9	0	0.7	4	0	0.8	4

^aSee Table 6. Reported values represent the number of rows (vertical distribution, maximum = 128) or columns (horizontal distribution, maximum = 26) containing at least one cell originally classified as a pool or ganglia element that persisted after simulated 2-day SEAR. Fifty realizations were analyzed for each simulation set.

Table 9. The 100-Day Natural Gradient Simulation Results for 50 Realizations in Each Ensemble

	Minimum	Mean	Maximum	Standard Deviation
Reference set				
Cumulative pore volumes	0.92	1.20	1.56	0.13
Effluent PCE concentration, ppm	66.9	111.7	142.9	18.9
Effluent PCE mass flux, g/d	18.3	37.5	60.0	8.5
Set 1				
Cumulative pore volumes	1.08	1.15	1.27	0.04
Effluent PCE concentration, ppm	73.0	112.4	141.3	18.0
Effluent PCE mass flux, g/d	22.6	36.1	48.7	6.3
Set 2				
Cumulative pore volumes	1.08	1.18	1.32	0.05
Effluent PCE concentration, ppm	82.7	112.7	140.6	14.1
Effluent PCE mass flux, g/d	27.3	37.4	50.0	5.3
Set 3				
Cumulative pore volumes	1.09	1.19	1.33	0.05
Effluent PCE concentration, ppm	62.7	113.6	145.2	25.3
Effluent PCE mass flux, g/d	21.1	37.9	54.5	8.89

[31] Independent realizations display a notably different relationship between flux-weighted PCE concentrations and percent PCE removed (Figure 8). These realizations exhibit more variability, but predict a reduction of one order of magnitude in PCE concentration after only 15–60% of the DNAPL is removed. Little further reduction in effluent concentration is then observed until more than 90% DNAPL is removed. For 90 to 99% DNAPL removal, correlated and independent realizations generally follow a similar path. Differences in the relationship between predicted concentration versus percent PCE recovery for correlated and independent realizations are attributable to differences in the initial and evolving DNAPL source zone architectures as discussed below.

4. Discussion

[32] A number of papers have demonstrated the ability of numeric multiphase flow models to simulate DNAPL

infiltration and entrapment in spatially variable porous media [e.g., *Kueper and Frind*, 1991a; *Essaid and Hess*, 1993; *Kueper and Gerhard*, 1995; *Dekker and Abriola*, 2000a; *Lemke et al.*, 2004]. These investigations have revealed the substantial influence of the spatial distribution of porosity, permeability, and capillary retention parameters on predicted immiscible flow pathways and organic spreading. *Dekker and Abriola* [2000b] illustrated the influence of variance and spatial correlation of the aquifer permeability field on remedial performance. To date, most researchers have relied on Gaussian spatially correlated random permeability fields, assumed constant porosity, and scaled capillary pressure-saturation curves to k using modified Leverett scaling in their investigations [e.g., *Kueper and Frind*, 1991b; *Kueper and Gerhard*, 1995; *Dekker and Abriola*, 2000a]. Such approaches generate irregular DNAPL saturation distributions that are qualitatively consistent with conceptual DNAPL source zone models and provide the means to evaluate flow and

Table 10. Two-Day SEAR Simulation Results for 50 Realizations in Each Simulation Set

	Minimum	Mean	Maximum	Standard Deviation
Reference set				
Cumulative pore volumes	9.70	12.7	16.5	1.39
PCE mass removed, kg	119.4	148.8	156.0	6.86
Percent PCE removal	76.7	95.4	100.0	4.36
Effluent PCE concentration, ppm	0.06	5.86	13.78	2.78
Effluent PCE mass flux, g/d	0.03	1.92	3.83	0.79
Set 1				
Cumulative pore volumes	11.4	12.2	13.5	0.48
PCE mass removed, kg	138.6	150.2	155.7	4.21
Percent PCE removal	88.9	96.3	99.8	2.67
Effluent PCE concentration, ppm	2.26	5.79	11.02	2.45
Effluent PCE mass flux, g/d	0.73	1.87	3.42	0.77
Set 2				
Cumulative pore volumes	11.4	12.5	14.0	0.57
PCE mass removed, kg	136.4	150.0	155.7	4.20
Percent PCE removal	87.6	96.2	99.8	2.67
Effluent PCE concentration, ppm	0.97	6.03	11.85	2.07
Effluent PCE mass flux, g/d	0.31	2.02	3.61	0.67
Set 3				
Cumulative pore volumes	11.4	12.5	14.0	0.57
PCE mass removed, kg	44.1	88.7	128.1	19.1
Percent PCE removal	28.7	57.3	82.4	12.3
Effluent PCE concentration, ppm	3.07	6.40	9.03	1.41
Effluent PCE mass flux, g/d	1.12	2.14	3.00	0.48

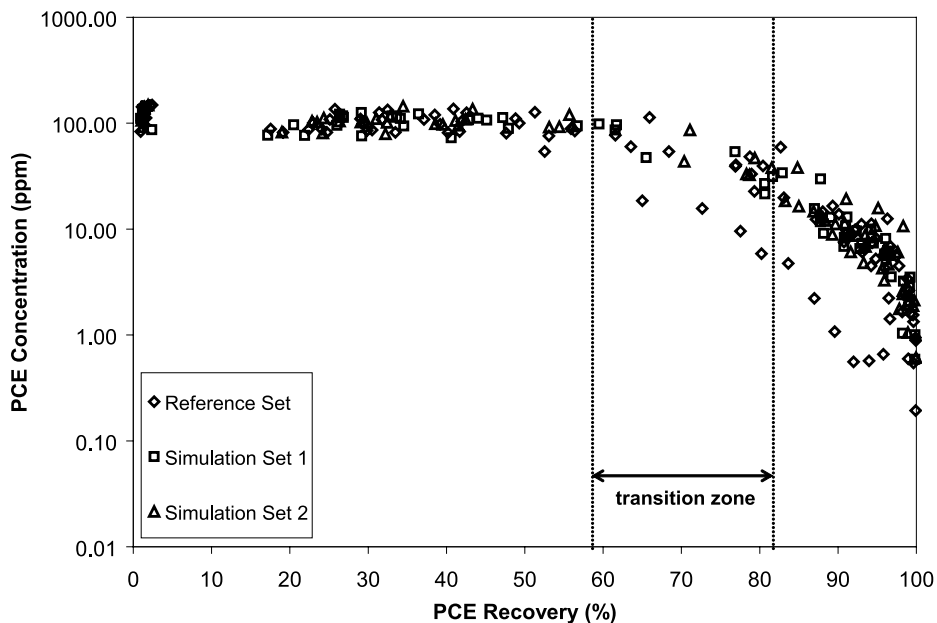


Figure 7. Flux-weighted effluent PCE concentrations versus PCE removal for representative realizations selected from correlated ensembles. Approximate one order of magnitude decrease in predicted PCE concentrations is associated with the transition from ganglia-dominated to pool-dominated source zone architecture illustrated in Figure 9. See color version of this figure in the HTML.

transport in nonuniform velocity fields. However, the application of Leverett scaling results in a perfect correlation between capillary entry pressure and permeability fields. Such a relationship has been shown to exert a controlling influence on predicted DNAPL spreading and redistribution in saturated aquifers [Lemke et al., 2002, 2004].

[33] Results of this investigation demonstrate that hydraulic property correlation also exerts an important influence on subsequent DNAPL recovery from homogeneous, nonuniform aquifers. Although the realizations in simulation sets 2 and 3 share identical porosity and permeability distributions, the correlated and independent ensembles behave differently under the conditions simulated.

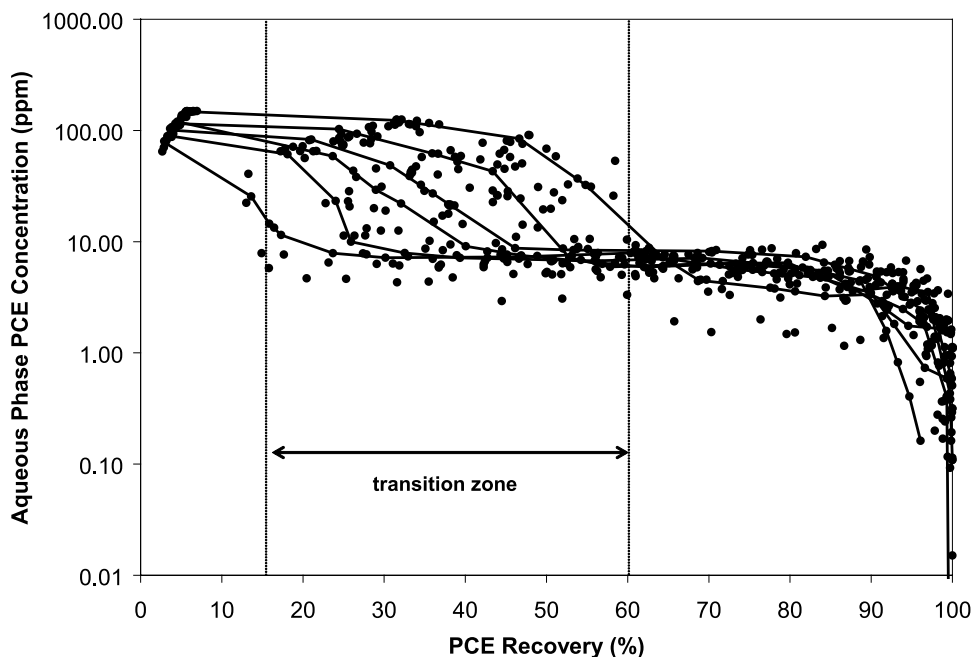


Figure 8. Flux-weighted effluent PCE concentrations versus PCE removal for 50 independent (set 3) realizations. Connected points show the path followed by six realizations chosen to illustrate variability in predicted concentration responses within the transition zone. See color version of this figure in the HTML.

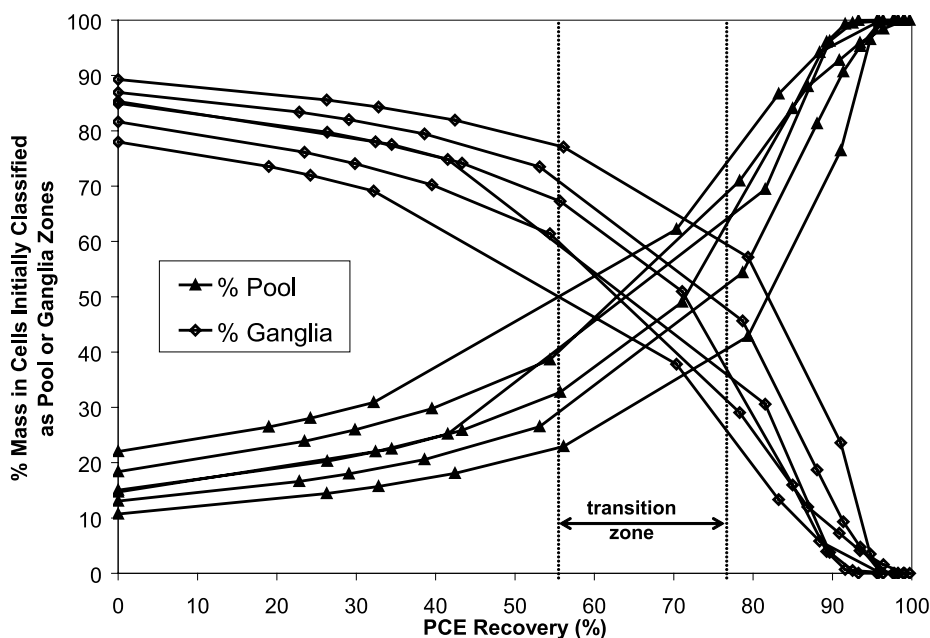


Figure 9. Mass fraction in cells initially classified as pool or ganglia versus percent PCE recovery for representative realizations from correlated set 2. See color version of this figure in the HTML.

In independent realizations, the correlation of P_b with grain size classes and the assignment of P_c -Sat parameters independently of the k field leads to a greater spatial continuity of similar entry pressure values that can account for the increased incidence of DNAPL pooling and higher maximum saturations [Lemke *et al.*, 2002]. As noted in section 3.3, the 2-day SEAR simulations predict that approximately 96% of PCE will be removed by surfactant flushing for correlated realizations. An equivalent surfactant flush removes approximately 60% of PCE in the independent ensemble due to a greater degree of pooling and higher entrapped DNAPL saturations. Nevertheless, the mean PCE mass flux following SEAR, predicted to decrease by one to two orders of magnitude relative to pre-SEAR conditions, was similar for all four ensembles investigated (Table 10). Plots of effluent PCE concentration as a function of percent PCE removed (Figures 7 and 8) indicate, however, that correlated and independent ensembles follow contrasting paths from similar initial to similar final conditions.

[34] Such differences in mass flux versus DNAPL removal behavior are attributable to differences in the evolution of the DNAPL source zone architecture in response to partial mass removal. Figure 9 illustrates changes in the relative proportion of DNAPL mass contained in cells classified as pools (regions exceeding the maximum residual organic liquid saturation, S_{or}) and ganglia (regions at or below S_{or}) for representative set 2 realizations (Table 3) as a function of DNAPL recovery. Pre-SEAR conditions are consistent with other correlated realizations: most mass is initially contained in cells with low organic liquid saturations classified as ganglia. With increasing PCE removal, the ratio of mass residing in cells initially classified as ganglia to mass residing in cells initially classified as pools decreases gradually until a crossover from ganglia-dominated to pool-dominated systems occurs between 65 and 90% PCE recovery. This “transition zone”

corresponds to the region of Figure 7 with an approximate one order of magnitude drop in effluent PCE concentrations.

[35] Figure 10 is a similar plot for representative independent set 3 realizations (Table 3). In this plot, pre-SEAR proportions of mass in pool and ganglia cells are more variable than those in correlated realizations (Figure 9). In general, however, more mass initially resides in pool elements than in ganglia elements. The transition zone coinciding with an approximate one-order drop in flux-weighted PCE concentrations (Figure 8) is reached after less removal of PCE mass for independent realizations than for correlated realizations (Figures 7 and 9). This transition occurs in response to lesser DNAPL mass removal (15 to 60% PCE recovery) in independent simulations because less PCE mass is initially contained in low-saturation ganglia cells and the contrast between organic saturations in pool and ganglia cells is greater. Less PCE mass distributed in approximately the same number of ganglia elements equates to lower average ganglia saturations in independent realizations. The earlier transition observed in independent realizations is therefore attributable to preferential removal of DNAPL mass from zones with lower organic saturation and generally higher relative permeability.

[36] Analogous behavior was observed in plots of PCE mass distributed in pool and ganglia cells for representative correlated and independent realizations simulated under natural gradient (0.001) flow conditions for a period of two decades (Figure 11). PCE mass initially contained in cells classified as ganglia decreases steadily with time for the correlated realizations selected from simulation set 2 while PCE mass in cells classified as pools remains relatively constant (Figure 11a). For the independent realizations selected from set 3 (Figure 11b), simulated PCE mass in cells classified as ganglia is removed sooner. Consequently, predicted PCE mass flux is more persistent over time in the correlated realizations compared to the independent realizations examined (Figure 12). Realization 36 from

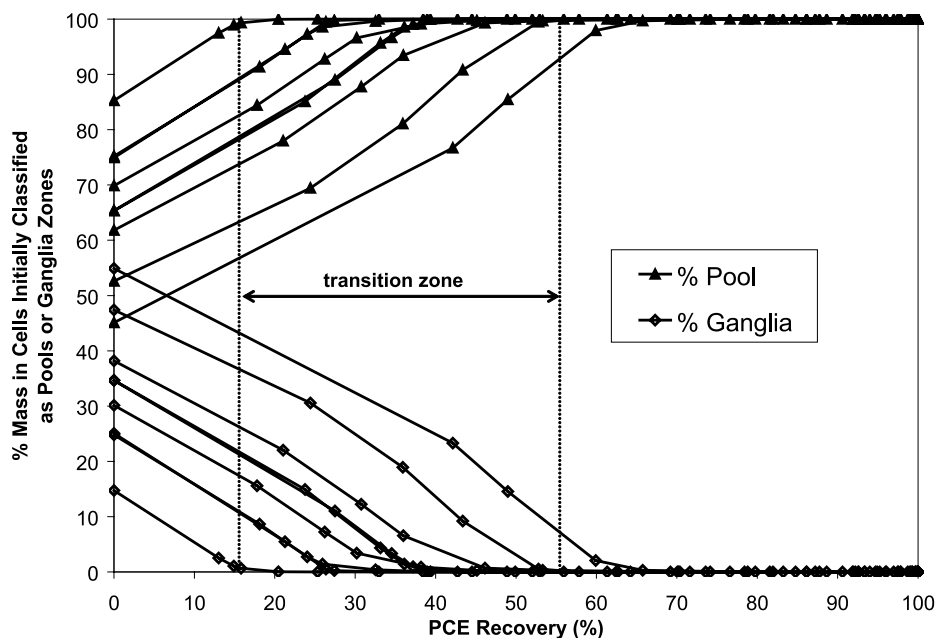


Figure 10. Mass fraction in cells initially classified as pool or ganglia versus percent PCE recovery for representative realizations from independent set 3. See color version of this figure in the HTML.

simulation set 2, which has the largest predicted organic liquid saturation (56.7%) among correlated realizations, behaved similarly to the independent realizations, all of which had higher organic saturations in the pool cells.

[37] In most aquifers, the dominant natural or engineered (water flood or surfactant flush) flow direction is horizontal. Under near-equilibrium or rate-limited mass transfer conditions in uniform flow fields, the majority of mass transfer from DNAPL to the aqueous phase can be shown to occur at the upstream edges of individual source subzones [Sale and McWhorter, 2001]. In laminar, nonuniform flow fields typical of most aquifers under natural gradient conditions, the highest rates of mass transfer are also likely to occur at the upstream edges of DNAPL source zones. Therefore the vertical distribution of DNAPL is a particularly important determinant of effluent mass flux and concentration when averaged over a vertical sampling interval such as a downgradient monitoring or extraction well. In the two-dimensional simulations considered here, the initial dissolution of PCE under natural gradient conditions resulted in flux-weighted concentrations on the order of 100 ppm across the downstream model boundary (Table 9). Values, ranging from 63 to 145 ppm, fell below the equilibrium PCE solubility limit (149 ppm) due to dilution caused by water flowing through uncontaminated portions of the profiles. The variation of initial concentrations is largely attributable to differences in the initial vertical distribution of ganglia elements (Table 7). Similarly, the relative persistence of the vertical distribution of pools following 2 days of simulated SEAR (Table 8) controls the position of plumes (Figures 1c and 2c) and the magnitude of dissolved PCE mass fluxes.

[38] Although each of the alternative approaches used to model capillary and hydraulic properties yielded irregular downward migration paths, pooling, and spreading that are qualitatively consistent with conceptual DNAPL source zone models, differences in pooled PCE saturations and

the fraction of mass residing in cells classified as pool versus ganglia were noted between correlated and independent ensembles. This study demonstrates that the same approaches also lead to different predictions of dissolved contaminant concentration and mass flux in response to DNAPL source zone mass removal of different degrees. The question of which approach is most appropriate is therefore important.

[39] The approach utilized to generate the independent set 3 ensemble is arguably more representative of the aquifer under study because the use of the SIS geostatistical method with categorical indicator classes incorporates more information from the original data set than direct simulation of k or K values using SGS. Specifically, spatial variability in contrasting grain size distribution (GSD) curve shapes is embedded in the distribution of geostatistical indicator classes. Because of the strong relationship between particle and pore size distributions in nonuniform sands, assignment of P_c -Sat parameters on the basis of indicator class distribution (e.g., using the *Haverkamp and Parlange* [1986] method) takes advantage of the GSD information embedded within those classes. Thus spatial continuity of simulated indicator classes is reflected in the spatial continuity of P_b estimates.

[40] Alternatively, it is difficult to find field or laboratory data for unconsolidated sediments supporting the relationship between P_b and k inherent in Leverett scaling. Published hydraulic conductivity and retention data do not support a strong correlation between entry pressures and k . For example, correlations for the log of saturated K values and van Genuchten alpha parameters measured in undisturbed and in situ soil samples reported by *Russo and Bouton* [1992] and *Hills et al.* [1992] were poor ($r^2 < 0.25$). Furthermore, if a representative retention curve is scaled to permeability, the P_b field is mapped directly onto the structure of the k field. NAPL spreading phenomena related to lateral continuity of vertically contrasting entry pressure

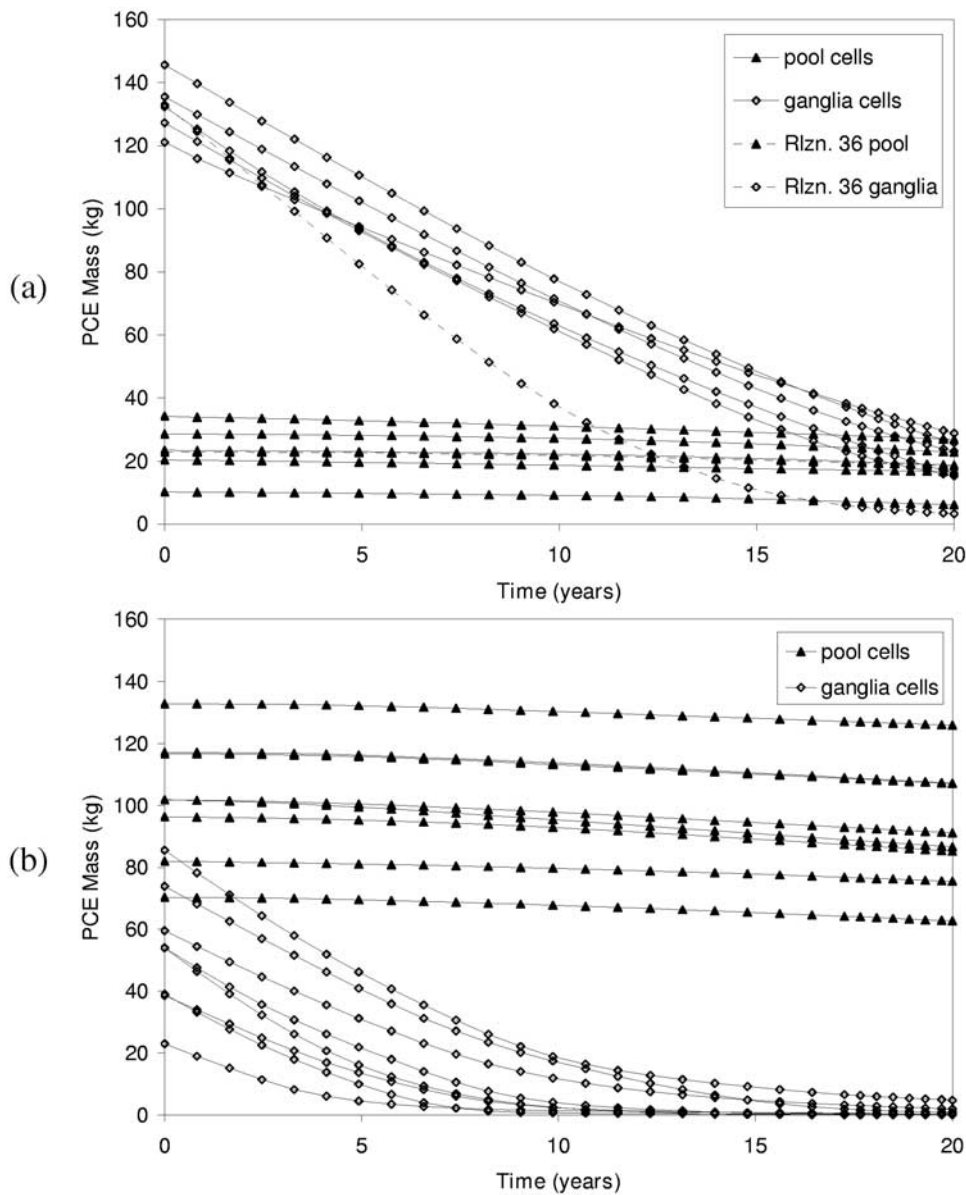


Figure 11. Persistence of PCE mass in pool and ganglia cells under natural gradient (0.001) conditions: (a) representative realizations from correlated simulation set 2 and (b) representative realizations from independent simulation set 3. See color version of this figure in the HTML.

values will be restricted to spatial locations with continuity in dissimilar k values. Because high saturations in PCE infiltration simulations are related to vertical contrast in P_b values (Figure 6), scaling P_b to Gaussian k fields may lead to underestimation of DNAPL pooling due to the inherent randomization of Gaussian geostatistical simulation processes [Journel and Deutsch, 1993; Gomez-Hernandez, 1997; Gomez-Hernandez and Wen, 1998].

[41] In heterogeneous or more highly nonuniform aquifers, however, such underestimation of DNAPL pooling may be less significant. PCE infiltration simulations conducted by Dekker and Abriola [2000a] using Gaussian K fields and Leverett-scaled entry pressures indicated a trend toward increasing organic liquid saturation and spreading with increasing $\sigma^2 \ln(K)$. For Leverett-scaled water wet sand systems with Gaussian K realizations, Phelan *et al.* [2004]

found that predicted aqueous phase effluent concentrations declined faster in response to percent PCE mass removal in realizations with increased $\sigma^2 \ln(K)$. This suggests that modification of simulated DNAPL source zone architecture in a way that increases pooling could lead to DNAPL recovery and contaminant flux behavior similar to that predicted here for independent realizations.

5. Summary and Conclusions

[42] Numerical studies of the type presented here provide insights into the influence of conceptual modeling decisions on numerical flow and transport model predictions. Lemke *et al.* [2004] demonstrated that differences in simulated pooling and entrapment behavior for spilled PCE resulted from alternative treatment of permeability and capillary

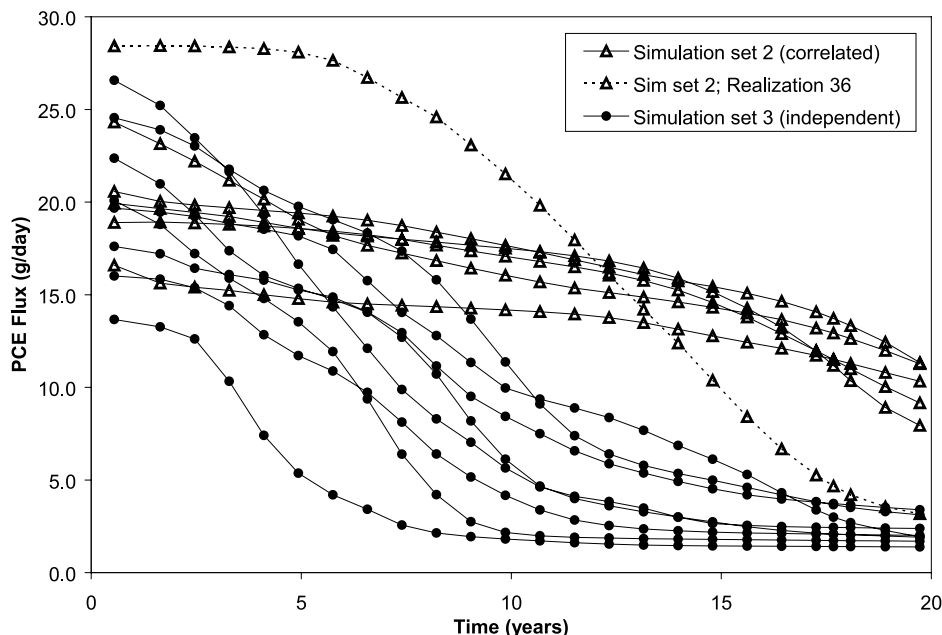


Figure 12. PCE flux versus time for representative realizations from correlated simulation set 2 and independent simulation set 3 simulated under natural gradient (0.001) conditions for 20 years. Flux measurements are summed across the effluent boundary of the model domain. See color version of this figure in the HTML.

entry pressure spatial correlation in a homogeneous, nonuniform aquifer. This study demonstrates that hydraulic property correlation also exerts an important influence on DNAPL recovery from the same aquifer.

[43] Using a simple working definition of pool and ganglia zones based on organic saturations relative to the maximum residual organic saturation defined along the main imbibition curve, the architecture of simulated DNAPL source zones was characterized with respect to the horizontal and vertical distribution of cells contributing to high initial aqueous phase mass flux under natural gradient conditions and persistent mass flux following simulated SEAR. For the alternative aquifer models considered in this study, it was observed that the removal of small fractions of the entrapped PCE did not change the source zone configuration. Consequently, predicted PCE effluent concentrations were not significantly reduced with respect to initial concentrations under natural gradient conditions until enough mass was removed to change DNAPL distributions from ganglia-dominated to pool-dominated. More PCE removal was required to effect this transition in ensembles constructed using Leverett scaling to determine the distribution of capillary entry pressures. In independent realizations, reductions in effluent PCE concentration of approximately one order of magnitude were predicted with as little as 20% DNAPL removal. Such disparities are attributable to differences in the initial distribution of PCE between pool and ganglia zones as well as to contrasts of average organic liquid saturations within pool and ganglia zones. After DNAPL removal in excess of 98%, the configuration and saturations of the few remaining cells containing organic were similar in all simulation sets, correlated and independent. Simulated DNAPL removal in excess of 99% of the original mass in place then became necessary before further reductions in dissolved phase concentrations were predicted.

[44] The results of this study support a growing understanding among researchers and environmental practitioners that a very large percentage of contaminant mass must be removed from DNAPL source zones before a reduction in aqueous phase concentrations below regulatory thresholds can be expected. However, they also demonstrate that benefits in the form of reduced mass flux can be accrued from partial source zone mass removal. Such benefits may not be readily apparent from analyses that rely on simplified conceptual models for DNAPL source zones or are unable to fully characterize the range of possible flow and dissolution phenomena associated with complex DNAPL source zone architectures and nonuniform flow fields. Additional simulations modeling aquifers with greater permeability variance and discretely heterogeneous permeability distributions are required before conclusions drawn here can be generalized to a wider range of aquifer conditions. Ultimately, however, detailed field measurements or controlled laboratory experiments likely will be required to demonstrate which of the different flux-weighted concentration responses to partial DNAPL source zone mass removal predicted by correlated and independent ensembles is most realistic.

[45] **Acknowledgments.** The U.S. Environmental Protection Agency, Great Lakes and Mid-Atlantic Center for Hazardous Substance Research (GLMAC-HSRC) under grant R-825540, the Michigan Department of Environmental Quality (MDEQ) under contract Y80011, and the Strategic Environmental Research and Development Program (SERDP) under contract CU-1293 provided funding for this research. The content of this manuscript has not been subject to agency review and does not necessarily represent the views of agency sponsors. This paper was improved by the thoughtful comments and questions provided by two anonymous reviewers.

References

Abriola, L. M., K. M. Rathfelder, S. Yadav, and M. Maiza (1992), VALOR code version 1.0: A PC code for simulating subsurface immiscible contaminant transport, *Rep. EPRI TR-101018*, Electr. Power Res. Inst., Palo Alto, Calif.

- Abriola, L. M., J. Lang, and K. Rathfelder (1997), Michigan soil-vapor extraction remediation (MISER) model—A computer program to model bioventing of organic chemicals in unsaturated geological material, *Rep. EPA/600R-97/099*, U.S. Environ. Prot. Agency, Washington, D. C.
- Abriola, L. M., C. D. Drummond, L. D. Lemke, K. M. Rathfelder, K. D. Pennell, E. K. Petrovskis, and G. Daniels (2001), Surfactant enhanced aquifer remediation: Application of mathematical models in the design and evaluation of a pilot-scale test, in *Natural and Enhanced Restoration of Groundwater Pollution*, edited by S. F. Thornton and S. E. Oswald, *IAHS Publ.*, 275, 303–309.
- Anderson, M. R., R. L. Johnson, and J. F. Pankow (1992), Dissolution of dense chlorinated solvents into groundwater: 3. Modeling contaminant plumes from fingers and pools of solvent, *Environ. Sci. Technol.*, 26, 901–908.
- Berglund, S. (1997), Aquifer remediation by pumping: A model for stochastic-advective transport with nonaqueous phase liquid dissolution, *Water Resour. Res.*, 33, 399–405.
- Brooks, R. H., and A. T. Corey (1964), Hydraulic properties of porous media, *Hydrol. Pap.* 3, Colo. State Univ., Fort Collins.
- Burdine, N. T. (1953), Relative permeability calculations from pore size distribution data, *Trans. Am. Inst. Min. Metall. Pet. Eng.*, 198, 71–78.
- Chrysikopoulos, C. V. (1995), Three-dimensional analytical models of contaminant transport from nonaqueous phase liquid pool dissolution in saturated subsurface formations, *Water Resour. Res.*, 31, 1137–1145.
- Dekker, T. J., and L. M. Abriola (2000a), The influence of field scale heterogeneity on the infiltration and entrapment of dense nonaqueous phase liquids in saturated formations, *J. Contam. Hydrol.*, 42, 187–218.
- Dekker, T. J., and L. M. Abriola (2000b), The influence of field scale heterogeneity on the surfactant-enhanced remediation of entrapped nonaqueous phase liquids, *J. Contam. Hydrol.*, 42, 219–251.
- Demond, A. H., and P. V. Roberts (1991), Effect of interfacial forces on two-phase capillary pressure-saturation relationships, *Water Resour. Res.*, 27, 423–437.
- Deutsch, C. V., and A. G. Journel (1998), *GSLIB Geostatistical Software Library and User's Guide*, 2nd ed., Oxford Univ. Press, New York.
- Drummond, C. D., L. D. Lemke, K. M. Rathfelder, E. J. Hahn, and L. M. Abriola (2000), Simulation of surfactant-enhanced PCE recovery at a pilot test field site, in *Treating Dense Nonaqueous Phase Liquids (DNAPLs): Remediation of Chlorinated and Recalcitrant Compounds*, edited by G. B. Wickramanayake, A. R. Gavaskar, and N. Gupta, pp. 77–84, Batelle, Monterey, Calif.
- Einarson, M. D., and D. M. Mackay (2001), Predicting impacts of groundwater contamination, *Environ. Sci. Technol.*, 35, 66A–73A.
- Essaid, H. I., and K. M. Hess (1993), Monte Carlo simulations of multiphase flow incorporating spatial variability of hydraulic properties, *Ground Water*, 31, 123–134.
- Essaid, H. I., W. N. Herkelrath, and K. M. Hess (1993), Simulation of fluid distributions observed at a crude oil spill site incorporating hysteresis, oil entrapment, and spatial variability of hydraulic properties, *Water Resour. Res.*, 29, 1753–1770.
- Feenstra, S., J. A. Cherry, and B. L. Parker (1996), Conceptual models for the behavior of dense non-aqueous phase liquids (DNAPLs) in the subsurface, in *Dense Chlorinated Solvents and Other DNAPLs in Groundwater: History, Behavior, and Remediation*, edited by J. F. Pankow and J. A. Cherry, pp. 53–88, Waterloo, Portland, Ore.
- Fountain, J. C. (1997), Removal of nonaqueous phase liquids using surfactants, in *Subsurface Restoration*, edited by C. H. Ward, J. A. Cherry, and M. R. Scaif, pp. 199–207, Ann Arbor Press, Chelsea, Mich.
- Fountain, J. C., R. C. Starr, T. Middleton, M. Beikirch, C. Taylor, and D. Hodge (1996), Controlled field test of surfactant-enhanced aquifer remediation, *Ground Water*, 34, 910–916.
- Freeze, R. A., and D. B. McWhorter (1997), A framework for assessing risk reduction due to DNAPL mass removal from low-permeability soils, *Ground Water*, 35, 111–123.
- Gomez-Hernandez, J. J. (1997), Issues on environmental risk assessment, in *Geostatistics Wollongong '96*, vol. 1, edited by E. Y. Baafi and N. A. Schofield, pp. 15–26, Kluwer Acad., Norwell, Mass.
- Gomez-Hernandez, J. J., and X.-H. Wen (1998), To be or not to be multi-Gaussian? A reflection on stochastic hydrology, *Adv. Water Resour.*, 21, 46–61.
- Haverkamp, R., and J. Y. Parlange (1986), Predicting the water-retention curve from particle-size distribution: 1. Sandy soils without organic matter, *Soil Sci.*, 142, 325–339.
- Hills, R. G., D. B. Hudson, and P. J. Wierenga (1992), Spatial variability at the Las Cruces trench site, in *Proceedings of the International Workshop on Indirect Methods for Estimating the Hydraulic Properties of Unsaturated Soils*, edited by M. T. van Genuchten, F. J. Leij, and L. J. Lund, pp. 529–538, Univ. of Calif., Riverside.
- Horvath, A. L. (1982), *Halogenated Hydrocarbons Solubility: Miscibility With Water*, Marcel Dekker, New York.
- Hunt, J. R., N. Sitar, and K. S. Udell (1988), Nonaqueous phase liquid transport and cleanup: 1. Analysis of mechanisms, *Water Resour. Res.*, 24, 1247–1258.
- Journel, A. G., and C. V. Deutsch (1993), Entropy and spatial disorder, *Math. Geol.*, 25, 329–355.
- Kueper, B. H., and E. O. Frind (1991a), Two-phase flow in heterogeneous porous media: 1. Model development, *Water Resour. Res.*, 27, 1049–1057.
- Kueper, B. H., and E. O. Frind (1991b), Two-phase flow in heterogeneous porous media: 2. Model application, *Water Resour. Res.*, 27, 1059–1070.
- Kueper, B. H., and J. I. Gerhard (1995), Variability of point source infiltration rates for two-phase flow in heterogeneous porous media, *Water Resour. Res.*, 31, 2971–2980.
- Kueper, B. H., W. Abbott, and G. Farquhar (1989), Experimental observations of multiphase flow in heterogeneous porous media, *J. Contam. Hydrol.*, 5, 83–95.
- Kueper, B. H., D. Redman, R. C. Starr, S. Reitsma, and M. Mah (1993), A field experiment to study the behavior of tetrachloroethylene below the water table: Spatial distribution of residual and pooled DNAPL, *Ground Water*, 31, 756–766.
- Lemke, L. D., L. M. Abriola, and P. Goovaerts (2002), Exploration of the influence of hydraulic property correlation on predictions of DNAPL infiltration and entrapment, in *Bridging the Gap Between Measurements and Modeling in Heterogeneous Media, Proceedings of the International Groundwater Symposium 2002*, edited by A. N. Findikakis, pp. 58–62, Int. Assoc. for Hydraul. Res., Delft, Netherlands.
- Lemke, L. D., L. M. Abriola, and P. Goovaerts (2004), DNAPL source zone characterization: Influence of hydraulic property correlation on predictions of DNAPL infiltration and entrapment, *Water Resour. Res.*, 40, W01511, doi:10.1029/2003WR001980.
- Leverett, M. C. (1941), Capillary behavior in porous solids, *Trans. Am. Inst. Min. Metall. Pet. Eng.*, 142, 152–169.
- National Research Council (NRC) (1994), *Alternatives for Groundwater Cleanup*, Natl. Acad. Press, Washington, D. C.
- Parker, J. C., and R. J. Lenhard (1987), A model for hysteretic constitutive relations governing multiphase flow: 1. Saturation-pressure relations, *Water Resour. Res.*, 23, 2187–2196.
- Pennell, K. D., A. M. Adinolfi, L. M. Abriola, and M. S. Diallo (1997), Solubilization of dodecane, tetrachloroethylene, and 1,2-dichlorobenzene in micellar solutions of ethoxylated nonionic surfactants, *Environ. Sci. Technol.*, 31, 1382–1389.
- Pennell, K. D., S. G. Pavlostathis, A. Karagunduz, and D. H. Yeh (2002), Influence of nonionic surfactants on the bioavailability of hexachlorobenzene for microbial reductive dechlorination, in *Chemicals in the Environment: Fate, Impacts, and Remediation*, edited by R. L. Lipnik et al., pp. 449–466, Oxford Univ. Press, New York.
- Phelan, T. J., L. D. Lemke, S. A. Bradford, D. M. O'Carroll, and L. M. Abriola (2004), Influence of textural and wettability variations on predictions of DNAPL persistence and plume development in saturated porous media, *Adv. Water Resour.*, 27, 411–427 doi:10.1016/j.advwtres.2004.02.011.
- Poulsen, M. M., and B. H. Kueper (1992), A field experiment to study the behavior of tetrachloroethylene in unsaturated porous media, *Environ. Sci. Technol.*, 26, 889–895.
- Powers, S. E., L. M. Abriola, and W. J. Weber, Jr. (1991), Theoretical study of the significance of nonequilibrium dissolution of nonaqueous phase liquids in subsurface systems, *Water Resour. Res.*, 27, 463–477.
- Powers, S. E., L. M. Abriola, and W. J. Weber, Jr. (1992), An experimental investigation of nonaqueous phase liquid dissolution in saturated subsurface systems: Steady state mass transfer rates, *Water Resour. Res.*, 28, 2691–2705.
- Powers, S. E., L. M. Abriola, and W. J. Weber, Jr. (1994), An experimental investigation of NAPL dissolution in saturated subsurface systems: Transient mass transfer rates, *Water Resour. Res.*, 30, 321–332.
- Ramsburg, C. A., and K. D. Pennell (2001), Experimental and economic assessment of two surfactant formulations for source zone remediation at a form dry cleaning facility, *Ground Water Monit. Rem.*, 21, 68–82.
- Rao, P. S. C., and J. W. Jawitz (2003), Comment on “Steady state mass transfer from single-component dense nonaqueous phase liquids in uniform flow fields” by T. C. Sale and D. B. McWhorter, *Water Resour. Res.*, 39(3), 1068, doi:10.1029/2001WR000599.
- Rao, P. S. C., J. W. Jawitz, C. G. Enfield, R. W. Falta, Jr., M. D. Annable, and A. L. Wood (2002), Technology integration for contaminated site

- remediation: Clean-up goals and performance criteria, in *Groundwater Quality: Natural and Enhanced Restoration of Groundwater Pollution*, edited by S. F. Thornton and S. E. Oswald, *IAHS Publ.*, 275, 571–578.
- Rathfelder, K. M., and L. M. Abriola (1998), Influence of capillarity in numerical modeling of organic liquid redistribution in two-phase systems, *Adv. Water Resour.*, 21, 159–170.
- Rathfelder, K. M., J. R. Lang, and L. M. Abriola (2000), A numerical model (MISER) for the simulation of coupled physical, chemical, and biological processes in soil vapor extraction and bioventing systems, *J. Contam. Hydrol.*, 43, 239–270.
- Rathfelder, K. M., L. M. Abriola, T. P. Taylor, and K. D. Pennell (2001), Surfactant enhanced recovery of tetrachloroethylene from a porous medium containing low permeability lenses 2, Numerical simulation, *J. Contam. Hydrol.*, 48, 351–374.
- Rathfelder, K. M., L. M. Abriola, M. A. Singletary, and K. D. Pennell (2003), Influence of surfactant-facilitated interfacial tension reduction on organic liquid migration in porous media: Observations and numerical simulation, *J. Contam. Hydrol.*, 64, 227–252.
- Russo, D., and M. Bouton (1992), Statistical analysis of spatial variability in unsaturated flow parameters, *Water Resour. Res.*, 28, 1911–1925.
- Saenton, S., and T. H. Illangasekare (2003), Evaluation of benefits of partial source zone treatment using intermediate-scale physical model testing and numerical analysis, in *Groundwater Engineering—Recent Advances, Proceedings of the International Symposium in Okayama, Japan, May 2003*, edited by I. Kono, M. Nishigaki, and M. Komatsu, pp. 25–35, A. A. Balkema, Brookfield, Vt.
- Saenton, S., T. H. Illangasekare, K. Soga, and T. A. Saba (2002), Effects of source zone heterogeneity on surfactant-enhanced NAPL dissolution and resulting remediation end-points, *J. Contam. Hydrol.*, 59, 27–44.
- Sale, T. C., and D. B. McWhorter (2001), Steady state mass transfer from single-component dense nonaqueous phase liquids in uniform flow fields, *Water Resour. Res.*, 37, 393–404.
- Schwille, F. (1988), *Dense Chlorinated Solvents in Porous and Fractured Media: Model Experiments*, A. F. Lewis, New York.
- Strategic Environmental Research and Development Program and Environmental Security Technology Certification Program (2002), SERDP/ESTCP Expert Panel Workshop on Research and Development Needs for Cleanup of Chlorinated Solvent Sites, final report, Arlington, Va.
- Stroo, H. F., M. Unger, C. H. Ward, M. C. Kavanaugh, C. Vogel, A. Leeson, J. A. Marqusee, and B. P. Smith (2003), Remediating chlorinated solvent source zones, *Environ. Sci. Technol.*, 37, 224A–230A.
- Taylor, T. P., K. D. Pennell, L. M. Abriola, and J. H. Dane (2001), Surfactant enhanced recovery of tetrachloroethylene from a porous medium containing low permeability lenses. 1. Experimental studies, *J. Contam. Hydrol.*, 48, 325–350.
- Taylor, T. P., K. M. Rathfelder, K. D. Pennell, and L. M. Abriola (2004), Effects of ethanol addition on micellar solubilization and plume migration during surfactant enhanced recovery of tetrachloroethylene, *J. Contam. Hydrol.*, 69, 73–99.
- Weber, W. J., and F. A. DiGiano (1996), *Process Dynamics in Environmental Systems*, John Wiley, Hoboken, N. J.
- Yeh, D. H., K. D. Pennell, and S. G. Pavlostathis (1999), Effect of Tween surfactants on methanogenesis and microbial reductive dechlorination of hexachlorobenzene, *Environ. Toxicol. Chem.*, 18, 1408–1416.

L. M. Abriola, Department of Civil and Environmental Engineering, Tufts University, Medford, MA 02155, USA.

J. R. Lang, Department of Civil and Environmental Engineering, University of Michigan, Ann Arbor, MI 48109, USA.

L. D. Lemke, Department of Geology, Wayne State University, Detroit, MI 48202, USA. (ldlemke@wayne.edu)